

Adaptive Guidance: Training-free Acceleration of Conditional Diffusion Models

Angela Castillo*¹ Jonas Kohler*² Juan C. Pérez*^{2,3} Juan Pablo Pérez¹
 Albert Pumarola² Bernard Ghanem³ Pablo Arbeláez¹ Ali Thabet²

¹Center for Research and Formation in Artificial Intelligence, Universidad de los Andes

²GenAI, Meta

³King Abdullah University of Science and Technology (KAUST)



Figure 1. **Accelerating Guided Diffusion Models with Adaptive Guidance:** By casting diffusion guidance as a Neural Architecture Search problem, we present Adaptive Guidance (AG), an efficient variant of Classifier-Free Guidance that saves 25% of total NFEs without compromising image quality. AG constitutes a training-free, plug-and-play alternative to Guidance Distillation that achieves 50% of its speed-ups while offering the ability to handle dynamic negative prompts. As depicted above, our approach (left) replicates the baseline one-to-one and furthermore outperforms a naïve reduction of diffusion steps (right).

Abstract

This paper presents a comprehensive study on the role of Classifier-Free Guidance (CFG) in text-conditioned diffusion models from the perspective of inference efficiency. In particular, we relax the default choice of applying CFG in all diffusion steps and instead search for efficient guidance policies. We formulate the discovery of such policies in the differentiable Neural Architecture Search framework. Our findings suggest that the denoising steps proposed by CFG become increasingly aligned with simple conditional steps, which renders the extra neural network evaluation of CFG redundant, especially in the second half of the denoising process. Building upon this insight, we propose “Adaptive Guidance” (AG), an efficient variant of CFG, that adaptively omits network evaluations when the denoising pro-

cess displays convergence. Our experiments demonstrate that AG preserves CFG’s image quality while reducing computation by 25%. Thus, AG constitutes a plug-and-play alternative to Guidance Distillation, achieving 50% of the speed-ups of the latter while being training-free and retaining the capacity to handle negative prompts. Finally, we uncover further redundancies of CFG in the first half of the diffusion process, showing that entire neural function evaluations can be replaced by simple affine transformations of past score estimates. This method, termed LINEARAG, offers even cheaper inference at the cost of deviating from the baseline model. Our findings provide insights into the efficiency of the conditional denoising process that contribute to more practical and swift deployment of text-conditioned diffusion models.

* Equal contributions.

1. Introduction

Diffusion Models (DMs) [14] exhibit outstanding generative capacities across domains such as images [45], video [15], audio [20], human pose estimation [5], and even cosmological simulations [48]. DMs generate data by sampling a noise instance and iteratively denoising the instance with a neural network. The sequential nature of this denoising operation makes sampling from DMs a slow and expensive process. In particular, the time required to sample from a given DM is a function of (i) the latency of each denoising iteration, and (ii) the total number of denoising steps.

Many practical applications entail “conditional generation”, where DMs create samples conditioned on specific criteria such as a class, a text, or an image [37]. DMs achieve conditional generation by replacing regular (*i.e.*, unconditional) denoising steps with conditional ones, in which the neural network processes both the input and the condition. While conditional denoising steps provide competitive results, Ho *et al.* proposed the technique of Classifier-Free Guidance (CFG) [13] to enhance sample quality. CFG enriches the conditional denoising process by leveraging implicit priors of the diffusion model itself. Despite its simplicity, CFG significantly improves sample quality in tasks such as text-to-image [8, 37, 40], image editing [4, 35, 50], and text-to-3D [26, 43]. Yet, the benefits of CFG come at the cost of *duplicating* the Number of Function Evaluations (NFEs), since each denoising iteration requires evaluating the neural network both conditionally and unconditionally. Adding to the problem, neural networks used in practice for DMs max out the parallelization capacity of production-grade GPUs¹, preventing simultaneous computation of the conditional and unconditional function evaluations.

In this paper, we improve the efficiency of text-to-image diffusion models that use Classifier-Free Guidance (CFG). Our analysis reveals that not all denoising steps contribute equally to image quality, suggesting that the traditional policy of applying CFG in all steps is sub-optimal. Instead, we search for policies offering more desirable trade-offs between quality and NFEs by employing techniques from differentiable Neural Architecture Search (NAS) [29]. Our NAS-based search suggests unnecessary computations take place in the latter part of the denoising process. We draw upon this finding, and propose an adaptive version of CFG that we call “Adaptive Guidance” (AG). Our AG policy is an efficient variant of CFG that enjoys the image quality of CFG despite requiring 25% fewer NFEs. Please refer to Fig. 1 for an illustration of the generation quality of AG.

¹By saturating memory bandwidth and/or CUDA cores. For example, using bfloat16 and batch size of 1, an EMU-768 model requires 1’553 ms on an A100 GPU without CFG. With CFG, latency almost doubles to 2’865 ms.

Compared to efficiency-oriented techniques like guidance distillation [36], AG is easy to implement, is training-free, and preserves the capacity to handle negative prompts. Finally, we propose LINEARAG, a fast version of AG that estimates updates required by AG as a linear combination of past iterates. LINEARAG provides further reductions in computation at the cost of imperceptible losses in sample quality.

In summary, our contributions are threefold:

- We show that techniques from gradient-based Neural Architecture Search (NAS) can be leveraged in the context of sampling from denoising diffusion models to discover efficient guidance policies.
- We propose an efficient and general plug-and-play alternative to Guidance Distillation that achieves 50% of the speed-ups while offering the ability to handle dynamic negative prompts and image editing.
- We discover that regularities across diffusion paths enable the replacement of certain NFEs in CFG with affine transformations of past iterates. This observation enables further runtime reductions and constitutes an interesting starting point for future research.

Find our full project and more resources on bcv.uniandes.github.io/adaptiveguidance-wp/.

2. Related Work

2.1. Fast Inference with Diffusion Models

Diffusion models [14, 38, 52] achieve density estimation and sampling by modeling a reversible transport map T that pushes forward a base distribution p_b that is tractable (usually a standard Gaussian) to a target distribution $p_*(\mathbf{x})$, *i.e.*, $T\#p_b = p_*(\mathbf{x})$. In contrast to traditional measure transport approaches (*e.g.*, [6, 10, 19]), diffusion models do not parameterize T explicitly but rather learn it implicitly from the reverse direction of a gradual noising process. This approach has the benefit of the transport T being learnable without the need for simulation. However, it also suffers from having higher inference costs due to the iterative nature of the sampling process.

Thus, a large body of work has focused on producing faster and more efficient ways of sampling from diffusion models. One angle of attack is the solver employed for integrating the differential equations that underlie the diffusion process. For example, methods based on exponential integrator [32, 33], higher order solvers [18, 58, 59] or model-specific

bespoke solvers [49, 60] have been proposed. Orthogonal to these efforts, [51] proposes parallelizing sampling via fixed-point iterations. Another common goal of exploration is reducing the size of the neural network that performs denoising [25, 40, 56]. For example, [56] explores ways of distilling a large teacher network into a smaller, more efficient, student. Yet, another set of papers explores ways of reducing the size of the diffusion’s latent space [12, 16, 44, 45]. Recently, a line of research explored reformulations of the diffusion process in order to reduce curvature in both the forward (noising) [1, 27] and backward (de-noising) trajectories [18, 21, 31, 42], which allows for larger solver steps even when employing lower-order solvers. Along these lines, [47] proposes to progressively reduce the number of diffusion steps by distillation.

Within the field of accelerating diffusion models, AutoDiffusion [24] is conceptually similar to our study in the sense that they employ a neural architecture search-inspired algorithm to improve the runtime of a pre-trained diffusion model. In contrast to AutoDiffusion, our method employs a more efficient gradient-based search instead of an evolutionary one. Furthermore, we optimize per-step guidance options, while AutoDiffusion focuses on time schedule and network architecture.

2.2. Conditioning Diffusion Paths

For both image generation and editing, the most challenging and practical cases involve some form of conditioning. Inspired by the success of class-conditioning in GANs (*e.g.*, [39]), [9] proposes to enhance the estimates of the diffusion probability path $p_t(\mathbf{x}|\mathbf{c})$ with the gradient of an image classifier $p_\theta(\mathbf{c}|\mathbf{x})$. Similarly, [37] proposes to use CLIP guidance for text-to-image generation with diffusion models. Yet, both approaches are prone to adversarial outcomes (*i.e.*, degenerate solutions) and struggle with the domain shift between the noisy images of the diffusion sampling process and the clean images on which the guidance models are trained.

In their seminal work, Ho *et al.* [13] show that the diffusion process can be successfully conditioned in a “classifier-free” manner by leveraging implicit priors of the diffusion model itself. Toward this end, Ho *et al.* jointly train a network to predict both unconditional and conditional scores. During generation, the two scores are combined, giving rise to the technique known as CFG, to pinpoint samples with high conditional probability, as given by the inverted diffusion model as implicit classifier². Unfortunately, by defini-

²While implicit classifiers are generally imperfect, especially when the model does not perfectly capture the data distribution (see [11], for in-

tion, the CFG scheme requires two, instead of one, NFEs per step, which doubles the sampling latency of the diffusion process on state-of-the-art models that max out GPU parallelization on a single sample.

Guidance Distillation (GD) [36] elegantly mitigates the need for an additional unconditional forward pass. However, GD requires re-training as well as re-evaluation, both of which are resource-intensive.³ Moreover, this technique cannot handle dynamic negative prompts, which are an important asset for responsible AI. It also does not work with compositional guidance [30], which is, for instance, used in text-to-3D generation [43]. Finally, it is unclear how to generalize GD to multimodal conditioning employed, for example, in image editing [4, 50].

In this work, we propose plug-and-play alternatives to Guidance Distillation that achieve 50% of the speed-ups at equal sample quality while conceptually omitting the aforementioned problems. For example, AG accommodates negative prompts (in Sec. 5), image editing (in Appendix B), is training-free, and exactly replicates the outputs of a given baseline such that no re-evaluation is needed.

2.3. Neural Architecture Search

Neural Architecture Search (NAS) aims at automating the design of neural network architectures by conceptualizing the network as a Directed Acyclic Graph (DAG) and exploring different layers as its nodes [3, 28, 41, 61, 62]. We focus this review on differentiable NAS methods [22, 23, 29, 55]. The DARTS framework [29] is particularly relevant to our work, as it introduces a continuous relaxation of the layer representation, allowing architecture search to be differentiable and, hence, more efficient. Here, we leverage analogies between neural network design and the diffusion process by unrolling the diffusion process’ graph in the time dimension, and thus considering each step as a distinct node in the DAG. This allows us to directly apply DARTS to search for an optimal guidance option at each node.

3. Background on Diffusion Models

As introduced in Sec. 2, diffusion models generate images by reversing a pre-defined noising process. In particular, when the noising process is an Ornstein-Uhlenbeck process, the continuous time limit of the forward SDE reads

(stance), the efficacy of CFG remains unambiguously evident in practice.

³To achieve comparable performance to CFG, Guidance Distillation on EMU-768 requires around 10k iterations with a batch size of 32, which amounts to roughly four GPU days on A100.

as $d\mathbf{x} = \mathbf{f}(\mathbf{x}, t) dt + g(t) d\mathbf{w}$, where $\mathbf{f}(\mathbf{x}, t) : \mathbb{R}^d \rightarrow \mathbb{R}^d$ is a vector-valued drift coefficient, $g(t) : \mathbb{R} \rightarrow \mathbb{R}$ is the diffusion coefficient of $\mathbf{x}(t)$ and \mathbf{w} is standard Brownian motion. Anderson’s Theorem [2] states that, under mild assumptions, this SDE satisfies a reverse-time process:

$$d\mathbf{x} = [\mathbf{f}(\mathbf{x}, t) - g(t)^2 \nabla_{\mathbf{x}} \log p_t(\mathbf{x})] dt + g(t) d\bar{\mathbf{w}}, \quad (1)$$

where $\bar{\mathbf{w}}$ is the reverse-time Brownian motion. As shown in [17, 54], the marginal transport map can be learned (in expectation) by maximum likelihood estimation of the scores of individually diffused data samples $\nabla_{\mathbf{x}} \log p_t(\mathbf{x})$ in a simulation-free manner. This map is commonly learnt by optimizing the parameters θ of a time-conditioned neural network that produces score estimates $\epsilon_{\theta}(\mathbf{x}_t, t)$.⁴

As shown in [54], the SDE in Eq. (1) has a deterministic counterpart (*i.e.*, an ODE) that enjoys equivalent marginal probability densities:

$$d\mathbf{x} = \left[\mathbf{f}(\mathbf{x}, t) - \frac{1}{2} g(t)^2 \nabla_{\mathbf{x}} \log p_t(\mathbf{x}) \right] dt. \quad (2)$$

Solving Eq. (2) generally yields better results when fewer discretization steps are taken [18].

Conditional generation with diffusion models. The diffusion framework can be extended to allow for conditional generation by learning the score $\log p_t(\mathbf{x}|\mathbf{c})$, where \mathbf{c} is, for example, a class- or text-condition. Current state-of-the-art models for conditional generation employ “Classifier-Free Guidance” (CFG) [13], a technique in which both the conditional and unconditional scores are linearly combined to denoise the sample. In particular, CFG proposes to follow the score estimate given by

$$\epsilon_{\text{cfg}}(\mathbf{x}_t, \mathbf{c}, s) = \epsilon_{\theta}(\mathbf{x}_t, \emptyset) + s \cdot (\epsilon_{\theta}(\mathbf{x}_t, \mathbf{c}) - \epsilon_{\theta}(\mathbf{x}_t, \emptyset)), \quad (3)$$

where \emptyset is the unconditional prompt token, and $s > 1$ indicates the guidance strength. While this new score may not directly reflect the gradient of a classifier’s log-likelihood, it is inspired by the gradient of an implicit classifier $p'(\mathbf{c}|\mathbf{x}) \propto p(\mathbf{x}|\mathbf{c})/p(\mathbf{x})$. As a result, $\nabla_{\mathbf{x}} \log p(\mathbf{c}|\mathbf{x}) \propto \nabla_{\mathbf{x}} \log p(\mathbf{x}|\mathbf{c}) - \nabla_{\mathbf{x}} \log p(\mathbf{x})$ and hence $\epsilon_{\lambda}(\mathbf{x}_t, \mathbf{c}) \propto \epsilon(\mathbf{x}_t, \emptyset) + s \cdot \nabla_{\mathbf{x}} \log p(\mathbf{x}|\mathbf{c})$. In that sense, CFG shifts probability mass toward data where an implicit classifier $p'(\mathbf{c}|\mathbf{x})$ assigns a high likelihood to the condition \mathbf{c} .

Notably, evaluating Eq. (3) introduces an extra NFE compared to unguided sampling, which may up to double the latency. Next, we search for efficient ways of guiding the denoising process, aiming at reducing NFES while retaining the benefits of CFG. In the following sections, we discuss these approaches along with their respective results.

⁴For brevity’s sake, we omit the conditioning of ϵ on t going forward.

4. Gradient Search along Diffusion Dynamics

Design space for guided diffusion steps. We assume access to a pre-trained diffusion model $\Phi : X \times C \rightarrow X$ working in latent space $X = \mathbb{R}^{H \times W \times C}$ and condition space C , where $\mathbf{c} \in C$ is a condition, *e.g.*, a text prompt. Initializing $\mathbf{x}_T \sim p_b$, where p_b represents a Gaussian distribution, setting a condition $\mathbf{c} \in C$ and a time-schedule $\tau = \{T, T-1, \dots, 0\}$, the diffusion model builds a sequence of latent codes

$$\{\mathbf{x}_t\}_{t=0}^T \text{ s.t. } \mathbf{x}_T \sim p_b, \mathbf{x}_{t-1} = \Phi(\text{solver}(\bar{\mathbf{x}}_t)), \quad (4)$$

where solver represents an ODE solver for Eq. (2). The model Φ operates under classifier-free guidance as given in Eq. (3), *i.e.*, $\bar{\mathbf{x}}_t = \epsilon_{\text{cfg}}(\mathbf{x}_t, \mathbf{c}, s)$ and s is constant over time. While this setup is the default in most popular diffusion models [8, 37, 45, 46], we highlight that multiple alternatives exist for $\bar{\mathbf{x}}_t$ at any given t , each associated with different computational costs:

- Unconditional score: $\epsilon_{\theta}(\mathbf{x}_t, \emptyset)$ (1 NFE)
- Conditional score: $\epsilon_{\theta}(\mathbf{x}_t, \mathbf{c})$ (1 NFE)
- CFG score: $\epsilon_{\text{cfg}}(\mathbf{x}_t, \mathbf{c}, s_t)$ (2 NFES)

Here, ϵ_{θ} represents a neural network parameterized by frozen weights θ , and s_t is no longer constant in time. Denote by f_t the particular step choice at time t with $f_t \in \mathcal{F}_t = \{\epsilon_{\theta}(\mathbf{x}_t, \emptyset), \epsilon_{\theta}(\mathbf{x}_t, \mathbf{c}), \epsilon_{\text{cfg}}(\mathbf{x}_t, \mathbf{c}, s_t)\}$. Then, the search space for the complete diffusion process is given by: $\mathcal{S} = \prod_{t=0}^T \mathcal{F}_t$, where the product symbol denotes the Cartesian product over sets.

As a result, \mathcal{S} is the set of all possible sequences of choices $\zeta = (f_0, f_1, \dots, f_T)$, which we henceforth refer to as *policies*. Clearly, \mathcal{S} is unbounded as long as $s_t \in \mathbb{R}$. Although this fact is not problematic in itself for gradient-based search, we constrain s_t to be in a bounded and finite set $\mathcal{S} = \{s^1, \dots, s^k\}$ in order to obtain simpler and more generalizable policies. As a result, the search spaces contain a total of $|\mathcal{S}| = |\prod_{t=0}^T \mathcal{F}_t| = (2+k)^{T+1}$ different policies.

Enabling backpropagation with soft alphas. Searching \mathcal{S} for policies with a good performance-latency trade-off constitutes a large-scale combinatorial problem, especially since T is usually in the range of 20 to 50. Thus, inspired by the literature on NAS, we relax the discrete search into a continuous one. This decision allows for effectively using gradients to navigate the high-dimensional search space. In particular, for each set of choices \mathcal{F}_t , we introduce a trainable vector $\alpha_t \in \mathbb{R}^{k+2}$ and obtain the solver input as a



Figure 2. **Adaptive Guidance (AG) vs. Classifier-Free Guidance (CFG) for multiple Number of Function Evaluations (NFEs).** For AG we keep the number of denoising iterations constant but reduce the number of steps using CFG by increasing the threshold $\tilde{\gamma}$ (top). CFG simply reduces the total number of diffusion steps (bottom). Vertically aligned samples require the exact same number of NFEs. As can be seen, AG replicates the baseline very closely while CFG with less steps introduces artifacts.

softmax weighting of the individual options

$$\bar{\mathbf{x}}_t := \text{softmax}(\boldsymbol{\alpha})^\top \mathcal{F}_t \quad (5)$$

Once trained, the score matrix $\boldsymbol{\alpha} := [\boldsymbol{\alpha}_T^\top, \dots, \boldsymbol{\alpha}_0^\top]$ represents a multinomial distribution over the per-iteration options $(\mathcal{F}_T, \dots, \mathcal{F}_0)$ from which we can sample concrete policies ζ . In the following, we define a differentiable objective to guide our search for efficient and effective guidance policies.

Search objective. We seek a policy ζ that gives rise to a diffusion model that replicates Φ as closely as possible, as quantified by a differentiable metric $d : X \times X \rightarrow [0, \infty)$ that measures the distance between the endpoints of the two diffusion paths (\mathbf{x}_0' and \mathbf{x}_0 , respectively). Our goal is to achieve replication with fewer NFEs than the reference policy $f_t = \epsilon_{cfg}(\mathbf{x}_t, \mathbf{c}, s)$, $\forall t$. Towards this end, we optimize:

$$\boldsymbol{\alpha}^* = \text{argmin}_{\boldsymbol{\alpha}} [d(\mathbf{x}_0, \mathbf{x}_0'(\zeta(\boldsymbol{\alpha})) + \lambda g(\zeta(\boldsymbol{\alpha}))], \quad (6)$$

where $\lambda > 0$ and $g(\zeta(\boldsymbol{\alpha}))$ regularizes the sum of the scores obtained by passing $\boldsymbol{\alpha}$ through a Gumbel-softmax [34] weighted by the per-choice costs (1 for unconditional/conditional steps and 2 for CFG steps with $s_t > 1$). Thus, g represents a (differentiable) proxy for the total NFEs of the policy $\zeta(\boldsymbol{\alpha})$. We employ a ReLU offset to a target cost limit \bar{c} under which no penalty is employed.

For the policy search, we initialize $\boldsymbol{\alpha}$ as i.i.d. uniform random variables. Subsequently, in each training iteration, we sample $\mathbf{x}_T \sim \mathcal{N}(0, I)$ and use our baseline model Φ to generate a target image \mathbf{x}_0 . The same starting noise tensor is then being fed through a student model Φ' that mimics Φ but employs a soft alpha-weighted forward pass according to Eq. (5) to obtain $\mathbf{x}_0'(\zeta(\boldsymbol{\alpha}))$. Given these two images, we compute the differentiable loss in Eq. (6) and backpropagate through Φ' w.r.t. $\boldsymbol{\alpha}$.⁵

4.1. Experimental Setup

We perform our guidance search in the context of text-to-image generation using the popular Stable Diffusion architecture [45], which we refer to as **LDM-512**.⁶ This model has 900M parameters and generates images at a 512×512 resolution via a latent space of shape $4 \times 64 \times 64$. To showcase that our findings generalize beyond the model they were searched on, we validate the found policies on a state-of-the-art EMU model [8], which we refer to as **EMU-768**. This model has 2.7B parameters, produces photorealistic images at a resolution of 768×768 , and uses a latent space

⁵To cope with limited memory resources, we re-run certain forward-pass segments during backward (“activation checkpointing”).

⁶We train LDM-512 from scratch on a commissioned dataset of images.

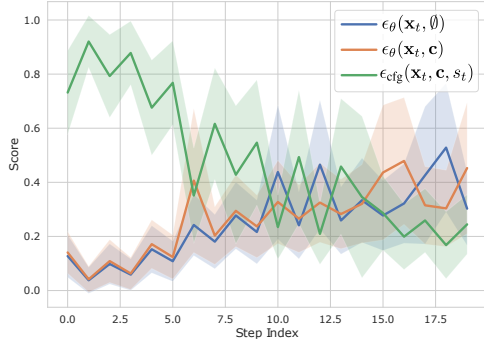


Figure 3. **Search results.** Average scores and standard deviations over steps in the diffusion process for the different guidance options. The 30 best searches are represented. As can be seen, CFG is most important in the beginning, and the score decreases over time.

of shape $16 \times 96 \times 96$.

For training, we generate 10,000 noise-image pairs randomly selected from the CC3M dataset [53] using our **LDM-512** with $T = 20$ DPM++ [32] solver steps and a fixed guidance strength of $s = 7.5$. In our search space \mathcal{S} we include $k = 3$ guidance strengths, which gives a total of five discrete choices: unconditional $\epsilon_\theta(\mathbf{x}_t, \emptyset)$, conditional $\epsilon_\theta(\mathbf{x}_t, \mathbf{c})$, as well as $\epsilon_{\text{cfg}}(\mathbf{x}_t, \mathbf{c}, a \cdot 7.5)$ for $a \in \{\frac{1}{2}, 1, 2\}$. We optimize Eq. (6) with the Lion optimizer [7] for 5 epochs. All evaluation metrics are computed on a subset of 1,000 prompts from the Open User Input (OUI) dataset [8].

4.2. Search Results

Upon completion of our search, we find that the best-performing policies focused essentially on three guidance choices: conditional, unconditional, and CFG with $s = 7.5$.⁷ The score distribution of these policies is summarized in Figure 3. Notably, a distinct pattern emerges in the search results: namely, the importance assigned to CFG is high in the first half of the denoising process but drops significantly in the second half. This fact follows intuition: text-conditioning is particularly important for determining the overall semantic structure of the image, and this semantic structure is set up early on in the diffusion process, while the later steps focus more on generating local information and high-frequency details (see *e.g.*, Fig. 17 in the Appendix).

Interestingly, this generative structure is mirrored in the inner workings of the diffusion process. Namely, the cosine similarity γ_t between the conditional ($\epsilon(\mathbf{x}_t, \mathbf{c})$) and un-

⁷In hindsight, this is not surprising as replicating a baseline model requires following the entire diffusion trajectory. Yet, by the design of the measured transport T , paths cannot cross, and there is no way of returning to the baseline once stepped off using a different guidance scale.

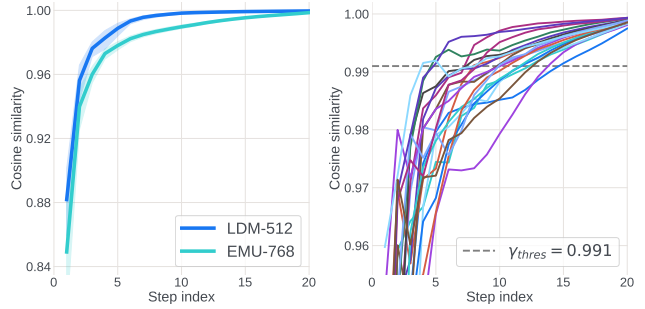


Figure 4. **Cosine similarities over time.** Left: Average cosine similarity γ and 99% confidence interval over 1,000 IOU prompts for EMU and LDM. Right: Zoom to y-values in $[0.955, 1.0]$ for 21 EMU samples.

conditional ($\epsilon(\mathbf{x}_t, \emptyset)$) network predictions increases almost monotonically over time. As shown in Fig. 4, γ_t achieves almost perfect alignment towards the end of the diffusion process. That is, we empirically observe

$$\lim_{t \rightarrow 0} \left[\gamma_t := \frac{\epsilon_\theta(\mathbf{x}_t, \mathbf{c}) \cdot \epsilon_\theta(\mathbf{x}_t, \emptyset)}{\|\epsilon_\theta(\mathbf{x}_t, \mathbf{c})\| \|\epsilon_\theta(\mathbf{x}_t, \emptyset)\|} \right] = 1. \quad (7)$$

In light of this finding, AG works because it stops guiding precisely when the conditional and unconditional update steps have converged, and guiding hence no longer introduces shifts in direction.

5. Adaptive Guidance

Definition. Section 4.2 found that the conditional and unconditional updates become increasingly correlated over time. This fact suggests an intuitive way to save NFEs by stopping CFG computation when this correlation is high. We thus expand on this intuition to propose ‘‘Adaptive Guidance’’ (AG), a principled technique to decrease sampling cost while maintaining high image quality. In particular, AG adaptively switches from CFG updates to (cheaper) conditional updates when γ_t (Eq. (7)) exceeds a threshold $\bar{\gamma}$, where $\bar{\gamma} \in [0, 1]$ is the only hyper-parameter of AG. As a result, AG results in uncomplicated policies such as

$\zeta_{\text{AG}} = [\epsilon_{\text{cfg}}(\mathbf{x}_T, \mathbf{c}), \dots, \epsilon_{\text{cfg}}(\mathbf{x}_t, \mathbf{c}), \epsilon_\theta(\mathbf{x}_{t-1}, \mathbf{c}), \dots, \epsilon_\theta(\mathbf{x}_0, \mathbf{c})]$, where the truncation point t is a function of $\bar{\gamma}$, the starting seed \mathbf{x}_T and the conditioning \mathbf{c} .

We highlight that ζ_{AG} is independent of the particular time schedule τ (Eq. (4)) and solver used for the sampling process. Hence, it can be within a wide class of diffusion models and for arbitrary numbers of diffusion steps. Importantly, as shown in Fig. 4, the cosine similarity trend found on LDM-512 generalizes to the much larger EMU-768 model.

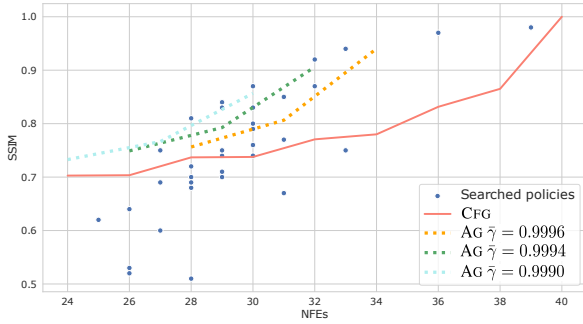


Figure 5. **Search results:** SSIM of different searched policies (dots) compared to the 20 step CFG baseline on LDM-512. Also depicted are results of AG for different truncation threshold $\bar{\gamma}$ (dashed lines) as well CFG with naïve step reduction (solid lines). The total number of steps reduces from right to left. As can be seen, AG is strictly better at replicating the baseline than a naïve step reduction. Furthermore, it matches most individual searched policies, while being simpler and scalable.

EMU-756	SSIM \uparrow	Win \uparrow	Lose \downarrow	NFEs \downarrow
CFG		502	498	40
AG $\bar{\gamma} = 0.991$	0.91 ± 0.03	498	502	29.6 ± 1.3

Table 1. **Evaluation results.** Comparison of AG ($\bar{\gamma} = 0.991$, approximately 30 NFE) and the 20 step (*i.e.* 40 NFE) CFG baseline. Avg. SSIM and majority voting of five trained human evaluators, each voting on 1,000 images generated from OUI prompts. AG achieves equal visual quality despite using 25% fewer NFEs.

Quantitative evaluation. We compare AG and CFG w.r.t. their capacity to reconstruct a set of 1,000 target images (computed from a baseline model with 20 CFG steps, *i.e.*, 40 NFEs). We run this experiment for LDM-512 and report results in Figure 5 for various values of $\bar{\gamma}$. We find that AG can replicate the target images to higher accuracy than CFG for the entire regime we considered (from 22 to 40 NFEs). Again, as detailed in Appendix A, these findings generalize to the much larger EMU-768 model.

Qualitative evaluation. Figure 2 depicts samples generated with AG for different $\bar{\gamma}$ values. Our results suggest that up to 50% of the diffusion steps can be performed without CFG at no cost to image quality. Moreover, Figures 1 and 2 showcase samples where AG outperforms the naïve alternative of reducing the total number of diffusion steps.

Human evaluation. We further validate AG’s capacity to generate images of CFG-level quality via a thorough human evaluation. Our assessment involved five trained human annotators, who were tasked with voting for the most visually appealing instance from a pair of images. One image was



Figure 6. **Human evaluation examples.** An exemplary sample for win (top) and lose (bottom) of AG with $\bar{\gamma} = 0.991$ vs. CFG. The baseline CFG tends to produce higher frequencies, which can be for better (bottom) or worse (top). We report further examples in Appendix A.

sampled from CFG (with 40 NFEs), and the other from AG with $\bar{\gamma} = 0.991$, inducing approximately a 25% reduction in NFEs. We ran this test on 1,000 prompts from the OUI dataset and report results in Table 1. Statistical analysis revealed a mean difference in votes of -0.047 ($SD = 2.543$), indicating no significant overall preference. The distribution of votes was nearly even, with AG favored in 498 cases and CFG in 502 cases (majority voting). We further conducted a two-sided Wilcoxon Signed-Rank Test, yielding a p -value of 0.603, with a test statistic of 244,590, indicating *no significant difference in visual appeal* between the two models ($p > 0.05$). These findings suggest that, despite the efficiency of AG, the generated images are of comparable quality to CFG, as judged by human annotators searching for visual aesthetics. Figure 13 depicts some exemplary samples of this evaluation.

5.1. Replacing NFEs with Affine Transformations

In the previous sections, we found that, in the latter stages of denoising, CFG updates can be replaced with conditional steps. Yet, for the first half of the denoising steps, guidance is of particular importance. Indeed, as shown in the first column of Fig. 8, reducing the number of guidance steps



Figure 7. **Negative prompts.** As can be seen, AG produces similar results to CFG when using non-empty negative prompts, again highlighting the importance of only the first $\frac{T}{2}$ diffusion steps for semantic structure. More such examples can be found in Figure 11 in the Appendix.

to as few as five (followed by 15 conditional steps) significantly degrades image quality. At the same time, the smooth alignment of conditional and unconditional steps over time and the high concentration around the mean of the cosine similarities depicted in Fig. 4 suggest a high regularity in diffusion paths. Intrigued by this observation, we probe for linear patterns in the diffusion path. Indeed, we find that unconditional network evaluations $\epsilon(\mathbf{x}_t, \emptyset)$ can often be estimated with high accuracy via *affine* transformations of network evaluations at previous iterations. To compute the parameters of these affine transformations, we generate a small dataset of 200 images from EMU-768 and store the intermediate iterations. Subsequently, we model a given unconditional step at any $t < T$ as a linear combination of the previous iterations in the diffusion chain as

$$\hat{\epsilon}(\mathbf{x}_t, \emptyset) = \sum_{i=T}^t \beta_i^c \epsilon_{\theta}(\mathbf{x}_i, \mathbf{c}) + \sum_{i=T}^{t+1} \beta_i^{\emptyset} \epsilon_{\theta}(\mathbf{x}_i, \emptyset), \quad (8)$$

where β_i^c and β_i^{\emptyset} are *scalars*. We learn these Linear Regression (LR) coefficients for each step by solving a simple Ordinary Least Squares problem on the set of 200 trajectories. Together with the time required for generating the dataset, we obtain LR coefficients for all steps in under 20 minutes. During sampling, computing $\hat{\epsilon}(\mathbf{x}_t, \emptyset)$ is essentially for free.

Perhaps surprisingly, we find that this estimator displays remarkable capacity to predict unconditional steps. Of course, for any unconditional score replaced by an LR predictor, the following denoising step will no longer have ground truth past information and errors accumulate autoregressively. Yet, interleaving CFG steps with “approximated” CFG steps (where the $\epsilon_{\theta}(\mathbf{x}_t, \emptyset)$ is replaced by its linear estimator $\hat{\epsilon}(\mathbf{x}_t, \emptyset)$), reduces the rate of error accumulation. We term this strategy LINEARAG. When $T = 20$, LINEARAG performs ten steps, alternating between CFG (2 NFEs) and LR-based CFG (1 NFE), followed by ten LR-based CFG steps. More details can be found in App. C.

As depicted in Fig. 8, LINEARAG drastically improves im-



Figure 8. **Replacing CFG in the first half of diffusion steps.** Three different approaches to reduce the number of NFEs in the first 50% of diffusion steps. As can be seen, LINEARAG samples show increased sharpness, dynamic lightning with higher contrast, and more vivid colors.

age quality over AG with very low $\bar{\gamma}$. Furthermore, it shows that the LR successfully recognizes patterns along the path since it compares favorably to the naïve alternative of simply alternating between CFG and conditional steps for the first half (followed by $\frac{T}{2}$ conditional steps). Finally, as reported in Figures 7 and 11, LINEARAG can even handle negative prompts to a certain extent.

6. Conclusions

In this paper, we have leveraged the gradient-based NAS framework to bring about principled insights into the denoising process of conditional diffusion models. In particular, we found that Classifier-Free Guidance involves computational redundancies of different sorts in both the first and second parts of the diffusion process. Leveraging these insights, we first proposed Adaptive Guidance, a very general and efficient plug-and-play variant of CFG that is able to closely replicate a baseline model while reducing the number of NFEs needed for guidance by up to 50%. Compared to Guidance Distillation, AG is training-free, extremely easy to implement and it offers considerable flexibility, for example when it comes to negative prompts or image editing.

Second, we proposed an even faster variant of CFG, termed LINEARAG, that increases the guidance NFE savings of AG to 75% by replacing entire network evaluations with surprisingly simple linear transformations of past information.

However, these extra runtime savings come at the price of LINEARAG no longer replicating the baseline one-to-one, which entails the need for extensive evaluations. As such, LINEARAG is to be considered more as a proof of concept as well as an interesting starting point for future research on finding ways to effectively leverage smoothness in and regularity across diffusion paths for efficient inference.

References

- [1] Michael S Albergo, Nicholas M Boffi, and Eric Vandenberg. Stochastic interpolants: A unifying framework for flows and diffusions. *arXiv preprint arXiv:2303.08797*, 2023. 3
- [2] Brian DO Anderson. Reverse-time diffusion equation models. *Stochastic Processes and their Applications*, 12(3):313–326, 1982. 4
- [3] Andrew Brock, Theodore Lim, James M Ritchie, and Nick Weston. Smash: one-shot model architecture search through hypernetworks. *arXiv preprint arXiv:1708.05344*, 2017. 3
- [4] Tim Brooks, Aleksander Holynski, and Alexei A Efros. Instructpix2pix: Learning to follow image editing instructions. In *Proceedings of the IEEE/CVF Conference on Computer Vision and Pattern Recognition*, pages 18392–18402, 2023. 2, 3, 1, 4
- [5] Angela Castillo, Maria Escobar, Guillaume Jeanneret, Albert Pumarola, Pablo Arbeláez, Ali Thabet, and Arsiom Sanakoyeu. Bodiffusion: Diffusing sparse observations for full-body human motion synthesis. *arXiv preprint arXiv:2304.11118*, 2023. 2
- [6] Ricky TQ Chen, Yulia Rubanova, Jesse Bettencourt, and David K Duvenaud. Neural ordinary differential equations. *Advances in neural information processing systems*, 31, 2018. 2
- [7] Xiangning Chen, Chen Liang, Da Huang, Esteban Real, Kaiyuan Wang, Yao Liu, Hieu Pham, Xuanyi Dong, Thang Luong, Cho-Jui Hsieh, et al. Symbolic discovery of optimization algorithms. *arXiv preprint arXiv:2302.06675*, 2023. 6
- [8] Xiaoliang Dai, Ji Hou, Chih-Yao Ma, Sam Tsai, Jialiing Wang, Rui Wang, Peizhao Zhang, Simon Vandenhende, Xiaofang Wang, Abhimanyu Dubey, et al. Emu: Enhancing image generation models using photogenic needles in a haystack. *arXiv preprint arXiv:2309.15807*, 2023. 2, 4, 5, 6
- [9] Prafulla Dhariwal and Alexander Nichol. Diffusion models beat gans on image synthesis. *Advances in neural information processing systems*, 34:8780–8794, 2021. 3
- [10] Laurent Dinh, Jascha Sohl-Dickstein, and Samy Bengio. Density estimation using real nvp. *arXiv preprint arXiv:1605.08803*, 2016. 2
- [11] Yves Grandvalet and Yoshua Bengio. Semi-supervised learning by entropy minimization. *Advances in neural information processing systems*, 17, 2004. 3
- [12] Shuyang Gu, Dong Chen, Jianmin Bao, Fang Wen, Bo Zhang, Dongdong Chen, Lu Yuan, and Baining Guo. Vector quantized diffusion model for text-to-image synthesis. In *Proceedings of the IEEE/CVF Conference on Computer Vision and Pattern Recognition*, pages 10696–10706, 2022. 3
- [13] Jonathan Ho and Tim Salimans. Classifier-free diffusion guidance. *arXiv preprint arXiv:2207.12598*, 2022. 2, 3, 4
- [14] Jonathan Ho, Ajay Jain, and Pieter Abbeel. Denoising diffusion probabilistic models. *Advances in neural information processing systems*, 33:6840–6851, 2020. 2
- [15] Jonathan Ho, William Chan, Chitwan Saharia, Jay Whang, Ruiqi Gao, Alexey Gritsenko, Diederik P Kingma, Ben Poole, Mohammad Norouzi, David J Fleet, et al. Imagen video: High definition video generation with diffusion models. *arXiv preprint arXiv:2210.02303*, 2022. 2
- [16] Jonathan Ho, Chitwan Saharia, William Chan, David J Fleet, Mohammad Norouzi, and Tim Salimans. Cascaded diffusion models for high fidelity image generation. *The Journal of Machine Learning Research*, 23(1):2249–2281, 2022. 3
- [17] Aapo Hyvärinen and Peter Dayan. Estimation of non-normalized statistical models by score matching. *Journal of Machine Learning Research*, 6(4), 2005. 4
- [18] Tero Karras, Miika Aittala, Timo Aila, and Samuli Laine. Elucidating the design space of diffusion-based generative models. *Advances in Neural Information Processing Systems*, 35:26565–26577, 2022. 2, 3, 4
- [19] Durk P Kingma and Prafulla Dhariwal. Glow: Generative flow with invertible 1x1 convolutions. *Advances in neural information processing systems*, 31, 2018. 2
- [20] Zhifeng Kong, Wei Ping, Jiaji Huang, Kexin Zhao, and Bryan Catanzaro. Diffwave: A versatile diffusion model for audio synthesis. *arXiv preprint arXiv:2009.09761*, 2020. 2
- [21] Sangyun Lee, Beomsu Kim, and Jong Chul Ye. Minimizing trajectory curvature of ode-based generative models. *arXiv preprint arXiv:2301.12003*, 2023. 3
- [22] Guohao Li, Guocheng Qian, Itzel C Delgadillo, Matthias Muller, Ali Thabet, and Bernard Ghanem. Sgas: Sequential greedy architecture search. In *Proceedings of the IEEE/CVF Conference on Computer Vision and Pattern Recognition*, pages 1620–1630, 2020. 3
- [23] Guohao Li, Mengmeng Xu, Silvio Giancola, Ali Thabet, and Bernard Ghanem. Lc-nas: Latency constrained neural architecture search for point cloud networks. In *2022 International Conference on 3D Vision (3DV)*, pages 1–11. IEEE, 2022. 3
- [24] Lijiang Li, Huixia Li, Xiawu Zheng, Jie Wu, Xuefeng Xiao, Rui Wang, Min Zheng, Xin Pan, Fei Chao, and Rongrong Ji. Autodiffusion: Training-free optimization of time steps and architectures for automated diffusion model acceleration. In *Proceedings of the IEEE/CVF International Conference on Computer Vision*, pages 7105–7114, 2023. 3
- [25] Yanyu Li, Huan Wang, Qing Jin, Ju Hu, Pavlo Chemerys, Yun Fu, Yanzhi Wang, Sergey Tulyakov, and Jian Ren. Snapfusion: Text-to-image diffusion model on mobile devices within two seconds. *arXiv preprint arXiv:2306.00980*, 2023. 3
- [26] Chen-Hsuan Lin, Jun Gao, Luming Tang, Towaki Takikawa, Xiaohui Zeng, Xun Huang, Karsten Kreis, Sanja Fidler, Ming-Yu Liu, and Tsung-Yi Lin. Magic3d: High-resolution text-to-3d content creation. In *Proceedings of the IEEE/CVF*

- Conference on Computer Vision and Pattern Recognition*, pages 300–309, 2023. 2
- [27] Yaron Lipman, Ricky TQ Chen, Heli Ben-Hamu, Maximilian Nickel, and Matt Le. Flow matching for generative modeling. *arXiv preprint arXiv:2210.02747*, 2022. 3
- [28] Chenxi Liu, Barret Zoph, Maxim Neumann, Jonathon Shlens, Wei Hua, Li-Jia Li, Li Fei-Fei, Alan Yuille, Jonathan Huang, and Kevin Murphy. Progressive neural architecture search. In *Proceedings of the European Conference on Computer Vision (ECCV)*, pages 19–34, 2018. 3
- [29] Hanxiao Liu, Karen Simonyan, and Yiming Yang. Darts: Differentiable architecture search. *arXiv preprint arXiv:1806.09055*, 2018. 2, 3
- [30] Nan Liu, Shuang Li, Yilun Du, Antonio Torralba, and Joshua B Tenenbaum. Compositional visual generation with composable diffusion models. In *European Conference on Computer Vision*, pages 423–439. Springer, 2022. 3
- [31] Xingchao Liu, Chengyue Gong, and Qiang Liu. Flow straight and fast: Learning to generate and transfer data with rectified flow. *arXiv preprint arXiv:2209.03003*, 2022. 3
- [32] Cheng Lu, Yuhao Zhou, Fan Bao, Jianfei Chen, Chongxuan Li, and Jun Zhu. Dpm-solver: A fast ode solver for diffusion probabilistic model sampling in around 10 steps. *Advances in Neural Information Processing Systems*, 35:5775–5787, 2022. 2, 6
- [33] Cheng Lu, Yuhao Zhou, Fan Bao, Jianfei Chen, Chongxuan Li, and Jun Zhu. Dpm-solver++: Fast solver for guided sampling of diffusion probabilistic models. *arXiv preprint arXiv:2211.01095*, 2022. 2
- [34] Chris J Maddison, Andriy Mnih, and Yee Whye Teh. The concrete distribution: A continuous relaxation of discrete random variables. *arXiv preprint arXiv:1611.00712*, 2016. 5
- [35] Chenlin Meng, Yutong He, Yang Song, Jiaming Song, Jiajun Wu, Jun-Yan Zhu, and Stefano Ermon. Sedit: Guided image synthesis and editing with stochastic differential equations. *arXiv preprint arXiv:2108.01073*, 2021. 2, 1
- [36] Chenlin Meng, Robin Rombach, Ruiqi Gao, Diederik Kingma, Stefano Ermon, Jonathan Ho, and Tim Salimans. On distillation of guided diffusion models. In *Proceedings of the IEEE/CVF Conference on Computer Vision and Pattern Recognition*, pages 14297–14306, 2023. 2, 3
- [37] Alex Nichol, Prafulla Dhariwal, Aditya Ramesh, Pranav Shyam, Pamela Mishkin, Bob McGrew, Ilya Sutskever, and Mark Chen. Glide: Towards photorealistic image generation and editing with text-guided diffusion models. *arXiv preprint arXiv:2112.10741*, 2021. 2, 3, 4
- [38] Alexander Quinn Nichol and Prafulla Dhariwal. Improved denoising diffusion probabilistic models. In *International Conference on Machine Learning*, pages 8162–8171. PMLR, 2021. 2
- [39] Augustus Odena, Christopher Olah, and Jonathon Shlens. Conditional image synthesis with auxiliary classifier gans. In *International conference on machine learning*, pages 2642–2651. PMLR, 2017. 3
- [40] William Peebles and Saining Xie. Scalable diffusion models with transformers. In *Proceedings of the IEEE/CVF International Conference on Computer Vision*, pages 4195–4205, 2023. 2, 3
- [41] Hieu Pham, Melody Y Guan, Barret Zoph, Quoc V Le, and Jeff Dean. Efficient neural architecture search via parameter sharing. *arXiv preprint arXiv:1802.03268*, 2018. 3
- [42] Aram-Alexandre Pooladian, Heli Ben-Hamu, Carles Domingo-Enrich, Brandon Amos, Yaron Lipman, and Ricky Chen. Multisample flow matching: Straightening flows with minibatch couplings. *arXiv preprint arXiv:2304.14772*, 2023. 3
- [43] Ben Poole, Ajay Jain, Jonathan T Barron, and Ben Mildenhall. Dreamfusion: Text-to-3d using 2d diffusion. *arXiv preprint arXiv:2209.14988*, 2022. 2, 3
- [44] Dominic Rampas, Pablo Pernias, Elea Zhong, and Marc Aubreville. Fast text-conditional discrete denoising on vector-quantized latent spaces. *arXiv preprint arXiv:2211.07292*, 2022. 3
- [45] Robin Rombach, Andreas Blattmann, Dominik Lorenz, Patrick Esser, and Björn Ommer. High-resolution image synthesis with latent diffusion models. In *Proceedings of the IEEE/CVF conference on computer vision and pattern recognition*, pages 10684–10695, 2022. 2, 3, 4, 5
- [46] Chitwan Saharia, William Chan, Saurabh Saxena, Lala Li, Jay Whang, Emily L Denton, Kamyar Ghasemipour, Raphael Gontijo Lopes, Burcu Karagol Ayan, Tim Salimans, et al. Photorealistic text-to-image diffusion models with deep language understanding. *Advances in Neural Information Processing Systems*, 35:36479–36494, 2022. 4
- [47] Tim Salimans and Jonathan Ho. Progressive distillation for fast sampling of diffusion models. *arXiv preprint arXiv:2202.00512*, 2022. 3
- [48] Andreas Schanz, Florian List, and Oliver Hahn. Stochastic super-resolution of cosmological simulations with denoising diffusion models. *arXiv preprint arXiv:2310.06929*, 2023. 2
- [49] Neta Shaul, Juan Perez, Ricky TQ Chen, Ali Thabet, Albert Pumarola, and Yaron Lipman. Bespoke solvers for generative flow models. *arXiv preprint arXiv:2310.19075*, 2023. 3
- [50] Shelly Sheynin, Adam Polyak, Uriel Singer, Yuval Kirstain, Amit Zohar, Oron Ashual, Devi Parikh, and Yaniv Taigman. Emu edit: Precise image editing via recognition and generation tasks. *arXiv preprint arXiv:2311.10089*, 2023. 2, 3, 1, 4
- [51] Andy Shih, Suneel Belkhale, Stefano Ermon, Dorsa Sadigh, and Nima Anari. Parallel sampling of diffusion models. *arXiv preprint arXiv:2305.16317*, 2023. 3
- [52] Jascha Sohl-Dickstein, Eric Weiss, Niru Maheswaranathan, and Surya Ganguli. Deep unsupervised learning using nonequilibrium thermodynamics. In *International conference on machine learning*, pages 2256–2265. PMLR, 2015. 2
- [53] Kaitao Song, Xu Tan, Tao Qin, Jianfeng Lu, and Tie-Yan Liu. Mass: Masked sequence to sequence pre-training for language generation. *arXiv preprint arXiv:1905.02450*, 2019. 6
- [54] Yang Song, Jascha Sohl-Dickstein, Diederik P Kingma, Abhishek Kumar, Stefano Ermon, and Ben Poole. Score-based

- generative modeling through stochastic differential equations. *arXiv preprint arXiv:2011.13456*, 2020. 4
- [55] Bichen Wu, Xiaoliang Dai, Peizhao Zhang, Yanghan Wang, Fei Sun, Yiming Wu, Yuandong Tian, Peter Vajda, Yangqing Jia, and Kurt Keutzer. Fbnet: Hardware-aware efficient convnet design via differentiable neural architecture search. In *Proceedings of the IEEE/CVF conference on computer vision and pattern recognition*, pages 10734–10742, 2019. 3
- [56] Xingyi Yang, Daquan Zhou, Jiashi Feng, and Xinchao Wang. Diffusion probabilistic model made slim. In *Proceedings of the IEEE/CVF Conference on Computer Vision and Pattern Recognition*, pages 22552–22562, 2023. 3
- [57] Kai Zhang, Lingbo Mo, Wenhui Chen, Huan Sun, and Yu Su. Magicbrush: A manually annotated dataset for instruction-guided image editing. *arXiv preprint arXiv:2306.10012*, 2023. 1
- [58] Qinsheng Zhang and Yongxin Chen. Fast sampling of diffusion models with exponential integrator. In *The Eleventh International Conference on Learning Representations*, 2022. 2
- [59] Wenliang Zhao, Lujia Bai, Yongming Rao, Jie Zhou, and Jiwen Lu. Unipc: A unified predictor-corrector framework for fast sampling of diffusion models. *arXiv preprint arXiv:2302.04867*, 2023. 2
- [60] Kaiwen Zheng, Cheng Lu, Jianfei Chen, and Jun Zhu. Dpm-solver-v3: Improved diffusion ode solver with empirical model statistics. In *Thirty-seventh Conference on Neural Information Processing Systems*, 2023. 3
- [61] Barret Zoph and Quoc Le. Neural architecture search with reinforcement learning. In *International Conference on Learning Representations*, 2016. 3
- [62] Barret Zoph, Vijay Vasudevan, Jonathon Shlens, and Quoc V Le. Learning transferable architectures for scalable image recognition. In *Proceedings of the IEEE conference on computer vision and pattern recognition*, pages 8697–8710, 2018. 3

Adaptive Guidance: Training-free Acceleration of Conditional Diffusion Models

Supplementary Material

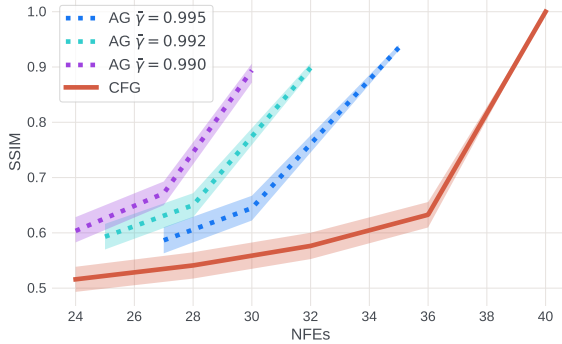


Figure 9. **AG vs CFG:** SSIM (mean and 95% CI) compared to the 20 step CFG baseline on EMU-768. Depicted are results of AG for different truncation threshold $\bar{\gamma}$ (dashed lines) as well as CFG with naive step reduction (solid lines). The total number of steps reduces from right to left. As can be seen, AG is strictly better at replicating the baseline than a naive step reduction. Similar results for LDM-512 can be found in Fig. 5

A. Evaluations on EMU-768

As stated in the main paper, our policy search was performed on the LDM-512 model. Importantly, we find that the resulting adaptive guidance policies generalize to the much bigger and more powerful EMU-768 model. For example 9, similar to Fig. 5 on LDM, shows that AG scales more favorably than CFG for different numbers of NFEs on EMU.

For our human evaluation results, we generated images using 20 CFG steps as well as 20 AG steps with $\bar{\gamma} = 0.991$, which gave rise to an average of 29.6 NFEs (that is, the average sample was generated with around 10 guided steps, followed by 10 unguided (conditional) steps). We used the same seed sequence for both models on a subset of 1000 prompts from OUI.

After generation, for each prompt, the images of both models were shown side-by-side to a random subset of 5 out of a pool of 42 trained human evaluators. The order of the images was also random. Annotators had to vote for higher visual appeal. There was no tie option to incentivize active engagement. The vote distribution was symmetric around zero (see Fig. 10). Hence, no significant difference in the model performance can be found by paired difference tests.

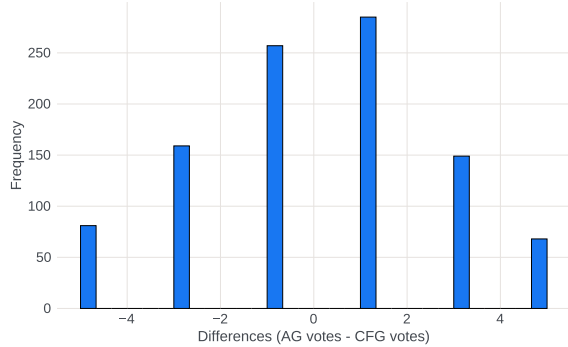


Figure 10. **Voting distribution.** Distribution of voting difference of five annotators for AG vs. CFG for 1000 samples. As can be seen, the distribution is very symmetric around zero. Hence, paired difference tests can find no significant difference in the model performance.

B. Image editing

A large body of works proposes to use text-to-image models not only for generation of novel images but also for instruction based editing of existing ones (e.g., [4, 35, 50, 57]). One particularly successful approach within this realm, termed InstructPix2Pix [4], achieve successful image editing by augmenting the CFG paradigm to not only text but image and text conditioning, giving rise to the modified score estimate

$$\begin{aligned} \epsilon_{\text{pix2pix}}(\mathbf{x}_t, \mathbf{c}, \mathbf{I}) = & \epsilon_{\theta}(\mathbf{x}_t, \emptyset, \emptyset) \\ & + s_c \cdot (\epsilon_{\theta}(\mathbf{x}_t, \mathbf{c}, \mathbf{I}) - \epsilon_{\theta}(\mathbf{x}_t, \emptyset, \mathbf{I})) \quad (9) \\ & + s_T \cdot (\epsilon_{\theta}(\mathbf{x}_t, \emptyset, \mathbf{I}) - \epsilon_{\theta}(\mathbf{x}_t, \emptyset, \emptyset)). \end{aligned}$$

This has two important implications. First, a single step in the diffusion process now requires 3 instead of 2 NFEs. Second, Guidance Distillation can no longer be applied as part of the “unconditional” update step is now dynamic (i.e., \mathbf{I} changes across samples, akin to the case of negative prompts).

Both effects are unfortunate as fast generation is particularly relevant in the image editing context, where users may want to try various instructions in sequence. Interestingly, we find that – similar to the case of simple text conditioning – the terms in Eq. 9 converge over time. Hence, as shown

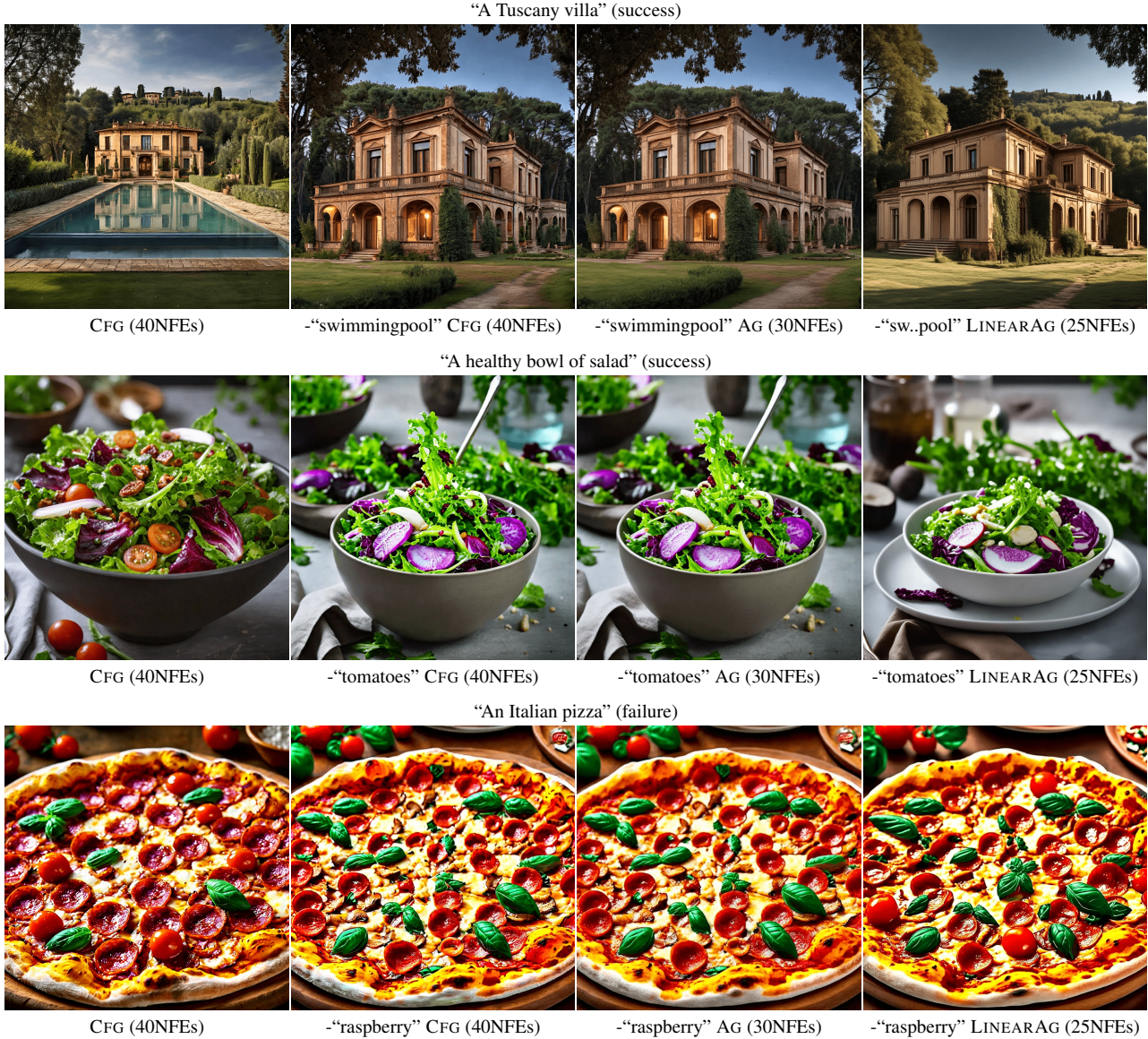


Figure 11. **More negative prompts.** More examples of using negative prompts with adaptive and linear adaptive guidance. The top and middle rows show successful examples. The bottom row shows a failure case. Importantly, standard CFG also fails in the latter case.

in Figure 14, AG can again be employed to reduce NFes without noticeable loss of quality. In the depicted images, AG employs only ten (instead of 20) $\epsilon_{\text{pix2pix}}(\mathbf{x}_t, \mathbf{c}, \mathbf{I})$ steps, thereby saving 33.3% of the total number of NFes.

C. OLS

In section 5.1, we have shown that entire neural network calls can be replaced by a simple linear regression in the past. This is particularly relevant for the first half of the diffusion steps, where we found guidance most important. Towards this end, we generated as little as 200 paths from

a 20-step CFG model and trained 20 linear regression models, one for each timestep, always taking the past unconditional as well as the past- and current conditional steps as regressors and the current unconditional as target. Importantly, we learned a single (scalar) regression coefficient for each high-dimensional regressor.⁸ The per-step errors of the learned LR models are depicted in Fig. 15.

After training the LR models, one can replace the unconditional network call $\epsilon_{\theta}(\mathbf{x}_t, \emptyset)$ in CFG with the simple linear

⁸Simple extensions like doing one OLS per channel did not show any significant improvement

“Two violins standing up with their bows on the ground” (win)



CFG (40NFEs)



AG, $\bar{\gamma} = 0.991$ (30NFEs)

“A toucan close up, midnight, lake, dark, moon light” (win)



CFG (40NFEs)



AG, $\bar{\gamma} = 0.991$ (30NFEs)

“three wolf moon but with cats instead of wolves” (win)



CFG (40NFEs)



AG, $\bar{\gamma} = 0.991$ (31NFEs)

“a realistic medieval castle built for bees in a sunflower field” (win)



CFG (40NFEs)



AG, $\bar{\gamma} = 0.991$ (29NFEs)

Figure 12. **Human evaluation examples (win)**. More samples from the human evaluation trials. The figure depicts a subset biased towards greater visual difference. We emphasize that images drawn uniformly from the dataset almost always look alike. This explains the draw situation depicted in Table 1.

“Fast commuter train moving past an outdoor platform.” (lose)



CFG (40NFEs)



AG, $\bar{\gamma} = 0.991$ (31NFEs)

“Three bears standing in a field outside.” (lose)



CFG (40NFEs)



AG, $\bar{\gamma} = 0.991$ (29NFEs)

“bee farm, The beatles, bees, honey, honey farm” (win)



CFG (40NFEs)



AG, $\bar{\gamma} = 0.991$ (30NFEs)

“two cats patting a magical crystal ball” (win)



CFG (40NFEs)



AG, $\bar{\gamma} = 0.991$ (30NFEs)

Figure 13. **Human evaluation examples (lose)**. More samples from the human evaluation trials. The figure depicts a subset biased towards greater visual difference. We emphasize that images drawn uniformly from the dataset almost always look alike. This explains the draw situation depicted in Table 1.



Figure 14. **Image editing.** Instruction based editing with EMU Edit [50], which builds upon InstructPix2Pix [4]. Depicted are the original image (left), classic CFG editing (Eq. 9) and AG editing, which gives equal quality results while reducing NFEs by 33.3%. Importantly, Guidance Distillation is not directly applicable for this task as the update steps are conditioned on the input image.

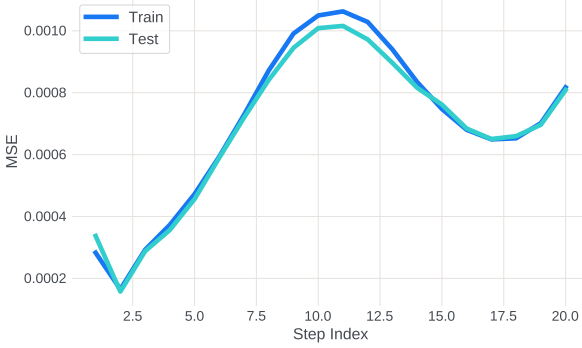


Figure 15. **Per-step OLS errors.** MSE of $\hat{\epsilon}(\mathbf{x}_t, \emptyset)$ and $\epsilon_\theta(\mathbf{x}_t, \emptyset)$ after learning the regression coefficients of Eq. 8. The results depict 200 training and 100 test samples.

combination $\hat{\epsilon}(\mathbf{x}_t, \emptyset)$ from Eq. 8, giving rise to

$$\hat{\epsilon}_{\text{cfg}}(\mathbf{x}_t, \mathbf{c}, s) = \hat{\epsilon}(\mathbf{x}_t, \emptyset) + s \cdot (\epsilon_\theta(\mathbf{x}_t, \mathbf{c}) - \hat{\epsilon}(\mathbf{x}_t, \emptyset)). \quad (10)$$

Importantly, this $\hat{\epsilon}_{\text{cfg}}$ update now only costs 1 NFE compared to the 2 NFEs for ϵ_{cfg} from Eq. 3.

We found that the LR estimators $\hat{\epsilon}(\mathbf{x}_t, \emptyset)$ can replace all unconditional network calls $\epsilon(\mathbf{x}_t, \emptyset)$ when given hypothetical ground truth past information. Of course, such information is no longer available once an upstream CFG step has been replaced with $\hat{\epsilon}_{\text{cfg}}$. Having observed that the regression weights β_i are highest for the most recent past, we found the best policy to be one that alternates between true CFG steps and LR-based CFG steps. For example, for the twenty-step baseline we are using the following policy

$$\zeta_{\text{LINEARAG}} = [\epsilon_{\text{cfg},T}, \hat{\epsilon}_{\text{cfg},T-1}, \epsilon_{\text{cfg},T-2}, \hat{\epsilon}_{\text{cfg},T-3}, \dots, \epsilon_{\text{cfg},T/2}, \hat{\epsilon}_{\text{cfg},T/2-1}, \hat{\epsilon}_{\text{cfg},T/2-2}, \dots, \hat{\epsilon}_{\text{cfg},0}]. \quad (11)$$

All LINEARAG results depicted in Fig. 8, 16 and 11 used ζ_{LINEARAG} .

“A painting of a gondola in the canals of 16th century Venice”



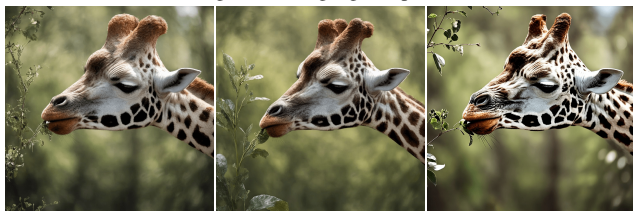
“A group of porcelain tucans painted in Inka style”



“An ancient castle on a cliff overlooking a vast, mist-covered valley”



“A giraffe eating a green plant”



AG $\bar{\gamma} = 0.975$
(25NFES)

naïve interleaving CFG
(25NFES)

LINEARAG
(25NFES)

Figure 16. **Replacing CFG in the first half of diffusion steps.** Three different approaches to reduce the number of NFES in the first 50% of diffusion steps. As can be seen, LINEARAG samples show increased sharpness, dynamic lightning with higher contrast, and more vivid colors. (Best viewed in zoom.)

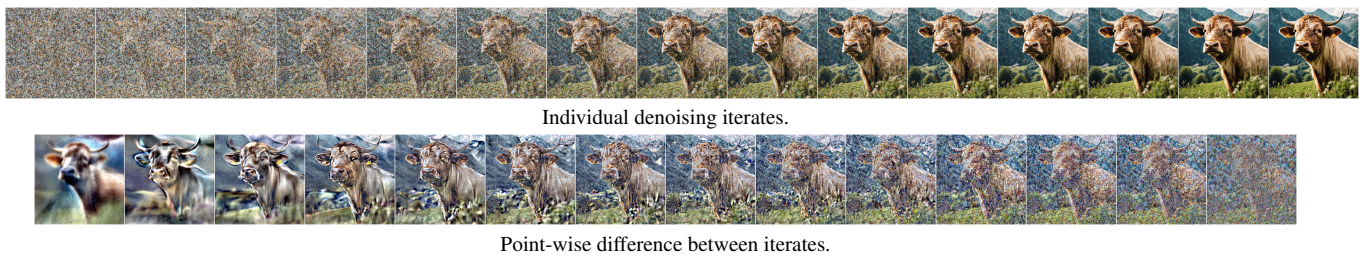


Figure 17. **Denoising process displays scene organization even in early iterations.** The (post-decoder) individual denoising iterates (top) suggest little information is known in the early iterations of the process. However, when computing the point-wise *differences* between the decoded iterates (bottom) shows that even the earliest iterations of the denoising process already display scene organization.